
Article:
Clements, A.G. orcid.org/0000-0003-3778-2248, Porter, R., Pranzitelli, A. et al. (1 more author) (2015) Evaluation of FSK models for radiative heat transfer under oxyfuel conditions. Journal of Quantitative Spectroscopy and Radiative Transfer, 151. pp. 67-75. ISSN 0022-4073

https://doi.org/10.1016/j.jqsrt.2014.09.019

Evaluation of FSK models for radiative heat transfer under oxyfuel conditions

Alastair G. Clements[a,*], Rachael Porter, Alessandro Pranzitelli[a], Mohamed Pourkashanian[a]

[a] *Energy Technology and Innovation Initiative, University of Leeds, Leeds, LS2 9JT, UK*

Abstract

Oxyfuel is a promising technology for carbon capture and storage (CCS) applied to combustion processes. It would be highly advantageous in the deployment of CCS to be able to model and optimise oxyfuel combustion, however the increased concentrations of CO_2 and H_2O under oxyfuel conditions modify several fundamental processes of combustion, including radiative heat transfer. This study uses benchmark narrow band radiation models to evaluate the influence of assumptions in global full-spectrum k-distribution (FSK) models, and whether they are suitable for modelling radiation in computational fluid dynamics (CFD) calculations of oxyfuel combustion. The statistical narrow band (SNB) and correlated-k (CK) models are used to calculate benchmark data for the radiative source term and heat flux, which are then compared to the results calculated from FSK models. Both the full-spectrum correlated k (FSCK) and the full-spectrum scaled k (FSSK) models are applied using up-to-date spectral data. The results show that the FSCK and FSSK methods achieve good agreement in the test cases. The FSCK method

*Corresponding author

Email address: pmagc@leeds.ac.uk (Alastair G. Clements)

Preprint submitted to Journal of Quantitative Spectroscopy & Radiative Transfer17th November 2018

using a five-point Gauss quadrature scheme is recommended for CFD calculations in oxyfuel conditions, however there are still potential inaccuracies in cases with very wide variations in the ratio between CO_2 and H_2O concentrations.
Keywords: Radiative transfer, Oxyfuel, Computational fluid dynamics, Full-spectrum k-distributions

1. Introduction

Oxyfuel is a promising technology to abate CO_2 emissions from combustion facilities. The process replaces air with high purity oxygen as the oxidant for fuel combustion. The oxygen supply is often diluted with recycled flue gas to control the flame temperature. The resulting flue gas from the oxyfuel process is composed entirely of the products from combustion, with a very high CO_2 concentration that can be purified to a level suitable for storage. Oxyfuel combustion has been successfully demonstrated at small scales [1–3], and there are further projects in development aiming to demonstrate the technology at much larger scales, such as the White Rose[1], FutureGen 2.0[2] and Youngdong projects.

There are several changes to the fundamental properties of combustion under oxyfuel, where the transparent and inert bulk gas N_2 is replaced with radiatively participating and potentially reactive CO_2 and H_2O. Furthermore, there are additional avenues of control available in the oxyfuel process, as the gas composition of the inlets is completely defined by the operator.

[1]http://www.whiteroseccs.co.uk/

[2]http://futuregenalliance.org/futuregen-2-0-project/

Drying or cooling the flue gas recycle, or changing the oxygen enrichment level, could result in drastic changes to the combustion process. In the development of oxyfuel technology it would be extremely useful to be able to accurately predict the influence of these changes to optimise the process, however models developed for predicting air-fired combustion may not be suitable for oxyfuel, with the models used for radiative heat transfer being repeatedly identified as a key area of research for oxyfuel modelling [4–6].

Radiation is the most significant thermal transfer mechanism at combustion temperatures. Failure to accurately account for the effects of thermal radiation will significantly affect further modelling predictions such as heat flux, gas velocity and species concentration predictions. The process of radiative transfer is influenced by the medium, where participating species, such as CO_2 and H_2O, will emit and absorb radiative energy. Accurate consideration of gas-phase radiation is important even in atmospheres where highly emissive particles, such as soot, are present due to strong self-absorption [7].

Combustion modelling has often made use of the grey weighted sum of grey gases (WSGG) method to account for gas absorption/emission in radiative transfer. The grey WSGG model has been successfully applied to air-fired combustion, but is only valid for predetermined environments, and the traditional models are unable to predict key radiative quantities in an oxyfuel environment [8, 9]. The full-spectrum k-distribution (FSK) models offer an alternative approach to accurately calculate radiative heat transfer for arbitrary gas mixtures, and can be evaluated fast enough to be applied in complex computational fluid dynamics (CFD) calculations [9, 10]. Previous modelling studies have shown a significant influence of using a FSK model in

CFD calculations, highlighting the need to accurately account for radiation heat transfer [7, 11, 12]. In addition to the FSK models that are the focus of this study, other global methods, such as the absorption distribution function (ADF) [13] and spectral line-based weighted sum of grey gasses (SLW) [14], are also potentially viable for calculating radiative transfer in novel environments within CFD calculations. These additional global models have been shown to be related to the FSK models [15, 16], and so the conclusions of this study may also be applicable to the ADF and SLW models.

This work focusses on the application and validation of FSK models to predict radiation heat transfer in oxyfuel environments within a commercial CFD code. The FSK models are validated against narrow-band predictions on a 3D enclosure that represents potential oxyfuel combustion environments. Calculations of the radiation energy source term and heat flux are compared between the benchmark narrow-band models, the standard grey WSGG model and the FSK models. A previous study identified FSK models as being accurate in potential air and oxyfuel cases [9]; this study updates the validation data and FSK parameters to recently developed spectral database values, and validates both the full-spectrum correlated k (FSCK) and full-spectrum scaled k (FSSK) models against two cases that test the underlying assumptions in the models for non-isothermal and non-homogeneous media. This study also identifies the optimal number of transfer equations that are required for the FSK models in the identified cases. The WSGG and FSK methods are implemented so that they are directly applicable to CFD calculations, allowing the conclusions from this study to be directly applicable to cases of practical interest.

2. Modelling radiative heat transfer

The directional radiative transfer equation (RTE) for an emitting, absorbing and non-scattering medium, assuming radiative equilibrium, is given as

$$\frac{\mathrm{d}I_\eta}{\mathrm{d}\hat{\mathbf{s}}} = \kappa_\eta(\underline{\phi})\left(I_{b\eta} - I_\eta\right) \tag{1}$$

where η denotes wavenumber, I_η is the spectral radiative intensity, $\hat{\mathbf{s}}$ is a ray direction through the medium, $I_{b\eta}$ is the spectral blackbody intensity, κ_η is the spectral absorption coefficient of the medium and $\underline{\phi}$ is a vector of the local gas properties that affect the absorption coefficient, namely pressure, temperature and gas composition. This study focuses on methods that evaluate the radiative intensity of a participating gas-phase medium, where absorption and emission are significant and scattering effects are negligible, so the RTE formulation in Equation (1) is adequate.

Radiation is coupled to the energy solution in CFD calculations through the radiation source term and the radiative heat flux. The radiation source term is the divergence of radiative heat flux through the medium, and can be calculated from the radiation intensity field as

$$\nabla \cdot \mathbf{q}_\mathrm{R} = \int_0^\infty \kappa_\eta(\underline{\phi})\left(4\pi I_{b\eta} - \int_{4\pi} I_\eta \,\mathrm{d}\Omega\right)\mathrm{d}\eta \tag{2}$$

where $\nabla \cdot \mathbf{q}_\mathrm{R}$ is the radiative source term, $\mathbf{q}_\mathrm{R}$ is the radiative heat flux at a position in the domain and Ω denotes solid angle. The radiation source term is important in calculating the temperature field, which has a significant impact on fluid dynamics and chemical reaction rates. The radiative contribution to the total heat flux at a surface can be calculated as

$$\mathbf{q}_\mathrm{R} \cdot \hat{\mathbf{n}} = \int_0^\infty \int_{4\pi} I_\eta \hat{\mathbf{s}} \cdot \hat{\mathbf{n}} \,\mathrm{d}\Omega \,\mathrm{d}\eta \tag{3}$$

where $\hat{\mathbf{n}}$ is the inward surface normal. Most of the surface heat flux in combustion systems is due to radiation, making the accurate treatment of this quantity important in evaluating the performance of the operating parameters for combustion.

Determining the quantities in Equations (2) and (3) across the whole spectral dimension is computationally expensive due to the variability of the absorption coefficient, which oscillates at very small spectral intervals – the exhaustive line-by-line (LBL) method typically requires over 10^6 RTE evaluations. The behaviour of the absorption coefficient for a potential oxy-fuel environment is shown in Figure 1. This study uses statistical narrow band (SNB) and correlated-k (CK) models to generate benchmark data to validate the global FSK models, which are also compared to the more standard grey WSGG model.

The SNB model is able to reach LBL accuracy in special cases within an acceptable time-frame, making it suitable for 3D calculations. The SNB model is often used to generate data for validating more time-efficient and widely-applicable models [9, 10, 17]. The CK model offers an alternative source of benchmark data to the SNB model, and the model provides a more amenable representation of absorption and emission, and is therefore applicable to more general RTE solvers. Global models, such as the WSGG and FSK models, calculate spectrally integrated values directly, allowing the solution to radiative transfer to be coupled with complex numerical simulations, as in CFD calculations, which is not viable with narrow-band models. This study validates the simplifying assumptions in the FSK models for oxyfuel conditions against the more accurate band models.

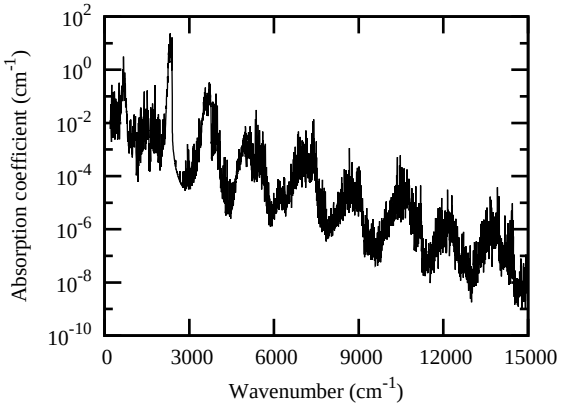

Figure 1: Absorption coefficient for a gas mixture of 85% CO_2, 10% H_2O and 5% N_2 at 1000K. Calculated from HITEMP2010 [18].

2.1. The statistical narrow-band model

The SNB model calculates radiation transfer based on averaged values across a narrow band, which are typically $\Delta\eta$=25cm^{-1} wide. The SNB model provides values for averaged band transmittance based on a statistical representation of the optical properties. For an isothermal and homogeneous path between s and s', the Malkmus [19] SNB model that is used in this study approximates the mean average transmittance across a narrow band as

$$\bar{\tau}_{s\to s'} = \exp\left[-\frac{2\bar{\gamma}}{\bar{\delta}}\left(\sqrt{1+\frac{\bar{k}\bar{\delta}xpl}{\bar{\gamma}}}-1\right)\right] \tag{4}$$

where $\bar{\gamma}$ is the mean spectral line Lorentz half-width, $\bar{\delta}$ is the mean line spacing, $\bar{k}$ is the mean intensity-to-spacing ratio, x is the absorbing species mole fraction, p is the pressure of the medium and l is the path length between s and s'.

To calculate the narrow-band intensity leaving a path defined by mean

transmittance, the discrete form of the narrow-band averaged RTE for black walls is given as [20]

$$\bar{I}_{\Delta\eta} \quad = \quad \bar{I}_{w\Delta\eta}\bar{\tau}_{\Delta\eta,1\to N+1} \; + \; \sum_{i=1}^{N} \bar{I}_{b\Delta\eta,i+1/2}\left(\bar{\tau}_{\Delta\eta,i+1\to N+1} - \bar{\tau}_{\Delta\eta,i\to N+1}\right) \quad (5)$$

where $\bar{I}_{\Delta\eta}$ is the narrow-band averaged intensity, $\bar{I}_{b\Delta\eta,i+1/2}$ is the narrow-band averaged blackbody intensity between point i and $i+1$ along the path, $\bar{I}_{w\Delta\eta}$ is the narrow-band averaged intensity emitted from the boundary, where $i = 1$, and N is the number of discrete points along the path. The SNB model is ill-suited for calculating radiative transfer in scattering media or for cases with non-black walls, however in the cases that are considered in this study the SNB model is accurate enough to produce results that can be considered a very good representation of the radiation field.

This work used a ray-tracing approach similar to the method described by Liu [17] to calculate the radiative source term and heat flux for a three-dimensional enclosure. The radiative intensity at a control surface is calculated by tracing a number rays from the centre of the surface to the boundary, and calculating the intensity propagating from the boundary back towards the control surface, using Equation (5). Discrete segments of the rays are defined as sections that are entirely inside one control volume, and were considered uniform with respect to the values calculated for the centre of the control volume. Non-homogeneous and non-isothermal paths were calculated using the Curtis-Godson approximation [21], which introduces a scaled assumption across narrow-band intervals. The radiative source term, $\nabla \cdot \mathbf{q}_{\mathrm{R}}$, was calculated using a first-order finite difference scheme. The number and direction of the rays were defined by a T_{N} quadrature set [22]. The sensitiv-

ity of the solution to the angular quadrature set was tested by running the calculation on increasing T_{N} sets until the solution was consistent with the next two sets. This method was chosen as it accurately represents the RTE, however it is noted that the implementation is not optimised for efficiency [17].

2.2. The correlated-k model

The CK model calculates narrow-band intensity through a reordered absorption coefficient across the band. By transforming the RTE to be defined as a function of a reordered distribution, which is chosen to be a smooth increasing function, it is possible to calculate band-averaged quantities using an efficient and accurate numerical quadrature scheme. The k-distribution across a narrow-band, $f(\underline{\phi}, k)$, is defined as

$$f(\underline{\phi}, k) = \frac{1}{\Delta\eta} \int_{\Delta\eta} \delta \left(k - \kappa(\underline{\phi}) \right) \mathrm{d}\eta \tag{6}$$

where δ is the Dirac delta function. The k-distribution represents the frequency that the absorption coefficient takes on a certain value, which is denoted as k in Equation (6). The narrow bands are chosen so that the blackbody intensity is practically constant across the band, so that its variations can be neglected. By taking the cumulative function of the k-distribution, defined as

$$g(\underline{\phi}, k) = \int_0^k f(\underline{\phi}, k') \, \mathrm{d}k' \tag{7}$$

it is possible to describe the k-distributions with a function bound between zero and one. The cumulative distribution $g(\underline{\phi}, k)$ represents the fraction of the narrow band with an absorption coefficient less than k.

The RTE for narrow-band intensity using the CK model is presented as

$$\frac{\mathrm{d}\bar{I}_{\Delta\eta,g_i}}{\mathrm{d}\hat{\mathbf{s}}} = k_{\Delta\eta}(\underline{\phi}, g_i)\left(I_{b\eta_0} - \bar{I}_{\Delta\eta,g_i}\right) \tag{8}$$

where $\bar{I}_{\Delta\eta,g_j}$ is the band-averaged intensity at g-space value g_j, $I_{b\eta_0}$ is the blackbody intensity evaluated at the band centre and $k_{\Delta\eta}(\underline{\phi}, g_i)$ is the re-ordered absorption coefficient in g-space, the inverse of the function shown in Equation (7). Using a suitable quadrature scheme, the total intensity can be evaluated as

$$\int_0^\infty I_\eta \,\mathrm{d}\eta \approx \sum_n^{N_b} \Delta\eta_n \sum_i^{N_q} w_i I_{n,i} \tag{9}$$

where N_b is the number of spectral bands, N_q is the number of quadrature points and w_i is the quadrature weight associated with point i.

The reordering operation introduced in Equation (6) is not strictly valid for different values of $\underline{\phi}$, and therefore the k-distribution method cannot be applied to inhomogeneous media without a simplifying approximation of the absorption coefficient. Introducing a correlated assumption for the absorption coefficient within a narrow band, the differences in $k(\underline{\phi}, g_j)$ between the g-space dimension of different thermodynamic states are neglected [23]. The introduction of the correlated assumption complements the scaled assumption introduced to the SNB model with the Curtis-Godson approximation.

In this work, the CK model parameters presented by Rivière and Soufiani [24] are used, which describe 51 narrow bands with a seven-point quadrature scheme, resulting in 357 RTE evaluations. The mixing scheme by Modest and Riazzi [25] is used to approximate k-distributions for gas mixtures from the single-specie CK model parameters. As the CK model describes the absorption properties of the gas directly, it can be used with the same RTE

solver as the FSK methods.

2.3. Full-spectrum k-distribution models

Similarly to the CK model, the FSK models calculate total intensity with a reordered absorption coefficient. The FSK model uses k-distributions across the entire spectrum, which are weighted by the Planck function to account for the variations in blackbody emissivity, as it can no longer be considered constant,

$$f(\underline{\phi}, T, k) = \frac{1}{I_b(T)} \int_0^\infty I_{b\eta}(T, \eta) \delta \left(k - \kappa(\underline{\phi}) \right) \mathrm{d}\eta \tag{10}$$

where $f(\underline{\phi}, T, k)$ is the full-spectrum k-distribution, I_b is the total blackbody intensity integrated across the spectrum and δ is the Dirac delta function. To facilitate integration, the spectral dimension is normalised, and redefined as the cumulative k-distribution at a reference state;

$$g_0(T_0, \underline{\phi}_0, k) = \int_0^k f(T_0, \underline{\phi}_0, k') \, \mathrm{d}k' \tag{11}$$

where g_0 is the cumulative k-distribution at a reference state $\underline{\phi}_0$ and reference temperature T_0. As with the CK model, the reordering operation in deriving the full-spectrum k-distribution results in the spectral dimension of two states not being directly related, and the absorption coefficient is required to be treated as either scaled or correlated across the entire spectrum. This treatment of the absorption coefficient is the main source of error in FSK models [26].

As it was mentioned for the CK model, it can be shown that the cumulative k-distribution for two correlated states is the same, and the RTE can be integrated across g_0 [26]. Employing this assumption, the RTE for an

emitting and absorbing medium can be rewritten for the FSCK model as

$$\frac{\mathrm{d}I_g}{\mathrm{d}\hat{\mathbf{s}}} = k^*(T_0, \underline{\phi}, g_0)\left[a(T, T_0, g_0)I_b(T) - I_g\right] \tag{12}$$

where

$$I_g = \frac{\int_0^\infty I_\eta \delta(k - k_\eta)\,\mathrm{d}\eta}{f(T_0, \underline{\phi}_0, k)} \tag{13}$$

$$a(T, T_0, g_0) = \frac{f(T, \underline{\phi}_0, k)}{f(T_0, \underline{\phi}_0, k)} = \frac{\mathrm{d}g(T, \underline{\phi}_0, k)}{\mathrm{d}g_0(T_0, \underline{\phi}_0, k)} \tag{14}$$

and where k^* is the correlation function that relates the reference cumulative k-distribution to the local state. Due to the smooth k-g distribution, illustrated in Figure 2, the total radiative intensity can be integrated across g-space using an efficient Gauss quadrature scheme [27],

$$\int_0^\infty I_\eta\,\mathrm{d}\eta = \int_0^1 I_g\,\mathrm{d}g_0 \approx \sum_i^{N_q} w_i I_{gi} \tag{15}$$

where N_q is the number of quadrature points used in the integration, w_i is the Gauss quadrature weight associated with quadrature point i and I_{gi} is the intensity evaluated for quadrature point i.

Alternatively to the correlated assumption, the absorption coefficient could be assumed to be scaled. The variation of a scaled absorption coefficient at different states can be separated from the spectral variation,

$$\kappa(\eta, \underline{\phi}) = \kappa(\eta, \underline{\phi}_0)u(\underline{\phi}_0, \underline{\phi}) \tag{16}$$

where $u(\underline{\phi}_0, \underline{\phi})$ is a scalar function. Using k-distributions, u can be calculated using the implicit relation [26]

$$\int_0^1 \exp\left[-k(T_0, \underline{\phi}, g)s\right]\mathrm{d}g \quad = \quad \int_0^1 \exp\left[-k(T_0, \underline{\phi}_0, g_0)u(\underline{\phi}_0, \underline{\phi})s\right]\mathrm{d}g_0 \tag{17}$$

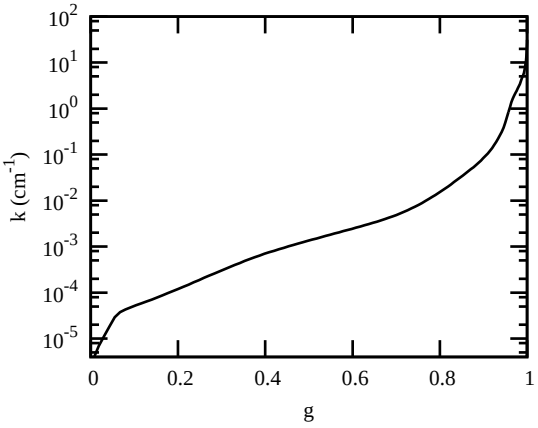

Figure 2: Full-spectrum k-g distribution calculated from the absorption coefficient in Figure 1.

where s is the mean beam length of the domain, which can be calculated using a commonly used relation based on the geometry [23]. In this work the mean beam length is calculated as $s = 3.6V/A$, where V is the internal volume of the domain and A is the bounding surface area. The integrations in Equation (17) can be evaluated using a Gauss quadrature scheme, and the relation can be effectively solved for the scaling function u by using a Newton-Raphson scheme [26]. Similarly to the FSCK model, the RTE for the FSSK model can be written as

$$\frac{\mathrm{d}I_g}{\mathrm{d}\hat{\mathbf{s}}} = k(T_0, \underline{\phi}_0, g_0)u(\underline{\phi}_0, \underline{\phi}) \left[a(T, T_0, g_0)I_b(T) - I_g\right] \tag{18}$$

The total intensity for the FSSK model can also be calculated using Equation (15).

It is important to select a representative reference state and temperature for the FSCK and FSSK models, as this is the only condition where both methods guarantee an exact solution. In this work the reference temperature

T_0 is also used for the reference state $\underline{\phi}_0$, and is calculated using the implicit relation [26]

$$\kappa_{\mathrm{PL}}(\underline{\phi}_0) I_b(T_0) = \frac{1}{V} \int_V \kappa_{\mathrm{PL}}(\underline{\phi}) I_b(T) \, \mathrm{d}V \tag{19}$$

where $\kappa_{\mathrm{PL}}(\underline{\phi})$ is the Planck-function weighted mean absorption coefficient at state $\underline{\phi}$. The mole fractions of the species for $\underline{\phi}_0$ are calculated as volume weighted averages across the domain. The reference pressure is set to atmospheric pressure as the cases in this study are all at constant atmospheric pressure.

The computational requirements of the FSCK and FSSK models are nearly identical, with the FSSK model only requiring a small increase in computational effort in the pre-processing step of calculating the scaling function [26]. Although the scaling approximation appears more constrictive, previous studies have shown that the predictions are often more accurate when the absorption coefficient is poorly correlated as Equation (14) provides a way to fit the k-distributions, which are truly neither scaled nor correlated, to the case being studied [26]. The most time-consuming part of the FSK models for CFD calculations is the number of RTEs that are required, which is dictated by the number of quadrature points used in Equation (15). It is important to choose the smallest number of points to ensure timely evaluation, while not sacrificing too much accuracy in the solution.

The calculation of the k-distributions used in Equation (12) and the scaling function in Equation (17) can be time-consuming to calculate from line-by-line data. To avoid this overhead it is possible to calculate the full-spectrum k-distributions for a gas mixture from narrow-band single-specie k-distributions with only a small loss in accuracy [25]. In this work the full-

spectrum k-distributions were calculated from a database generated by Cai and Modest [28] that was updated for the HITEMP2010 data [18], and is provided as part of the Spectral Radiation Calculation Software (SRCS). To further reduce the computational effort, the k-distributions, scaling functions and a functions were calculated in a pre-processing step, generating a look-up table for a series of predetermined values of $\underline{\phi}$ and T, and linear interpolation between these values was used when solving the RTE. The resolution of the lookup table was set to similar values to the resolution of the database, and increasing this resolution did not affect the solution. The mixing scheme by Modest and Riazzi [25] is used in this study to calculate the k-distributions of H_2O/CO_2 mixtures. The difference in the spectral data used to evaluate the benchmark and FSK data for CO_2 may introduce a source of error, however these errors should be small at the temperatures being considered in this study, which are below 2000K [29].

Both the correlated and scaled assumptions often break down in cases with large gradients in temperature [30] or relative species concentrations [27]. Under combustion conditions it is expected that there will be significant gradients in temperature at the flame edge, which could also coincide with significant variations in relative species concentrations. Specifically for oxyfuel, especially if the flue gas recycle is pre-dried, it is likely there will be areas with a high CO_2 concentration juxtaposed to a reaction zone producing a variable ratio of H_2O and CO_2. The approximations in the FSK models need to be validated against possible oxyfuel conditions before they can be applied with confidence.

3. Case descriptions

The test cases used in this study are similar to the cases previously proposed by Liu [17]. The radiative source term, Equation (2), and radiative heat flux, Equation (3), are solved for a 2m×2m×4m enclosure, that is bounded by black walls and contains a participating medium with a fixed composition and temperature.

The first case is the same as the case proposed by Porter et al. [9]. The enclosure contains a gas mixture that is 85% CO_2, 10% H_2O and 5% N_2 by volume, with a temperature profile that is non-uniform but symmetric around the centreline parallel to the z-axis. The centreline temperature is a piecewise linear profile that increases from 400K at z=0m, to 1800K at z=0.375m and then decreases to 800K at z=4m. The radial temperature distribution is defined as

$$T = \begin{cases} (T_c - 800)f(r) + 800 & r \leq 1 \\ 800 & r > 1 \end{cases} \tag{20}$$

where T_c is the centreline temperature, r is the distance of the location from the centreline and where $f(r) = 1 - 3r^2 + 2r^3$. The walls are kept at 300K. The temperature distribution is illustrated in Figure 3. The geometry is divided into a 17×17×24 cell grid, with a higher density of cells in the high temperature region, identical to the third case by Liu [17]. The SNB benchmark data in this work is updated with the new parameters from Rivière and Soufiani [24]. The T_6 quadrature scheme was used to generate the SNB benchmark data. Increasing the number of rays to the T_8 scheme did not significantly affect the solution.

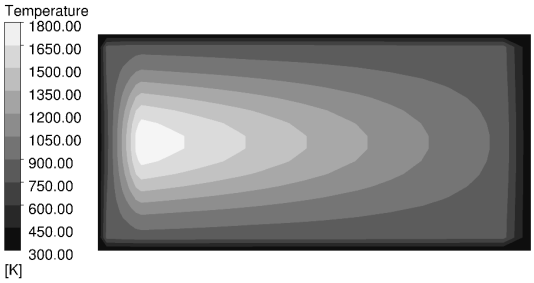

Figure 3: The temperature distribution in the first case on the Y=1m plane.

The second case is defined to represent a wide range of product species ratios that may occur under oxyfuel conditions. The temperature is uniform within the enclosure at 1500K, and the walls are black at 500K. The species distribution within the enclosure is non-uniform and varies so that the molar ratio of H_2O/CO_2 is bound between 0.125 and 2, with individual species defined as

$$X_{\mathrm{H_2O}} = 2\left(\frac{z}{4}\right)\left(1-\frac{z}{4}\right)+0.1 \tag{21}$$

$$X_{\mathrm{CO_2}} = 0.9 - X_{\mathrm{H_2O}} \tag{22}$$

$$X_{\mathrm{N_2}} = 0.1 \tag{23}$$

where X_{sp} is the mole fraction of species sp. The distribution of the mole fraction of CO_2 is illustrated in Figure 4. CO radiation was not considered in either case as the majority of the radiative heat flux and source term are expected to arise from interactions from CO_2 and H_2O, especially in oxyfuel cases with recycled flue gas. For the second case the geometry was divided into a uniform 11×11×25 cell grid. The T_8 quadrature scheme was used for the SNB results on the second case as there were noticeable differences between the T_6 and T_8 schemes, but not between the T_8 and T_{10} schemes.

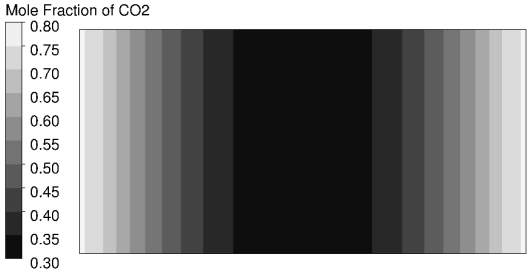

Figure 4: The CO_2 distribution in the second case on the Y=1m plane.

Each solution was obtained using the commercial CFD code ANSYS Fluent v14.5, incorporating user-defined functions to customise the radiation model. The benchmark SNB data were calculated within ANSYS Fluent v14.5 using an 'on-demand' user-defined function to ensure that the geometry was identical between the narrow-band and global models. The finite volume method (discrete ordinates) provided in ANSYS Fluent was used to calculate the CK model results, using an angular discretisation of $N_\theta = N_\phi = 3$. Increasing the angular discretisation to $N_\theta = N_\phi = 4$ did not alter the results. Due to the reasonably large spacial resolution, producing a relatively significant optical thickness for each control volume, the second-order upwind method was used to calculate control surface values.

For both cases, the FSCK and FSSK models were evaluated using a Gauss quadrature scheme, where the number of quadrature points were varied between three and nine, and were applied using the same finite volume method to solve the RTE as described with the CK model. For brevity, only the results for three, five and seven quadrature points in the FSK models are shown, as the solution did not change significantly for more than five points. Increasing the angular resolution did not alter the solutions. All of the cases

were run in serial on a 3 GHz CPU and took less than a couple of minutes to reach a converged solution for the FSK models, however there was a noticeable time penalty when applying a higher number of quadrature points. The results from the FSK models are also compared against the results from the grey WSGG model that is available in ANSYS Fluent v14.5, which is based on the coefficients by Smith et al. [31].

4. Results and discussion

The results for the first case are shown in Figures 5 and 6, illustrating the variation of the radiative source term along the centreline parallel to the z-axis and the surface radiative heat flux on the wall along the line (0m,1m,z). The results show that an optimal choice for the number of quadrature points lies around five points, as there is only a small change in the derived values as this number increases. The results of the SNB and CK models show a disagreement in peak regions.

Both of the FSK models demonstrate similar predictions for the radiative source term in the first case, with the FSCK and FSSK models (Figures 5a and 6a respectively) marginally under-predicting the magnitude of the source term with respect to the benchmark data. The FSCK and FSSK models also produce very similar results with regards to the radiative surface heat flux, shown in Figures 5b and 6b, over-predicting the values calculated with the narrow-band models. The very good agreement between the FSK models and the CK model supports the assessment that the discrepency between the benchmark data can be attributed to the different RTE solvers, and that the formulation of the global models does not sacrifice any accuracy in this case.

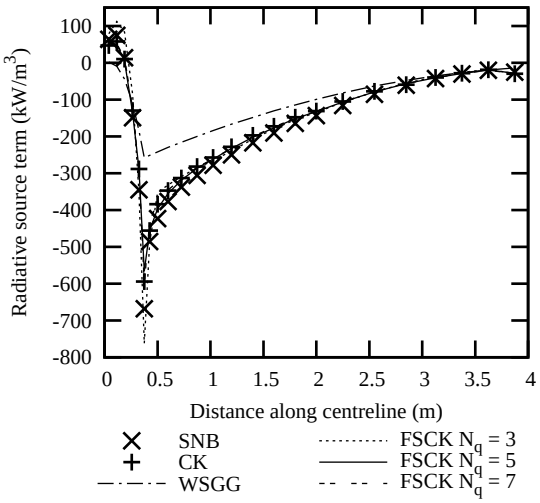

(a) Radiative source term calculations along the centreline.

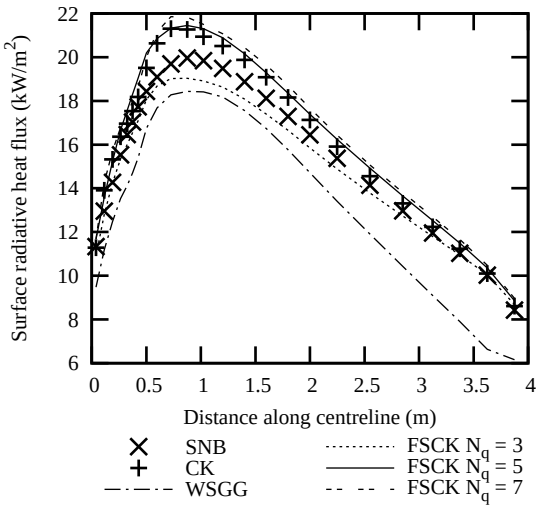

(b) Surface radiative heat flux calculations along the wall line (0m,1m,z).

Figure 5: Results for the FSCK on the first case.

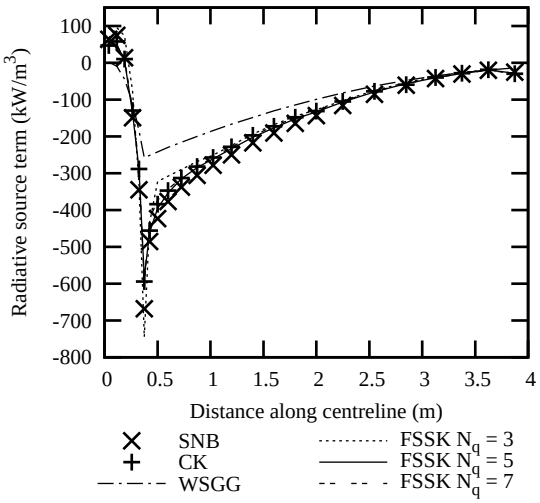

(a) Radiative source term calculations along the centreline.

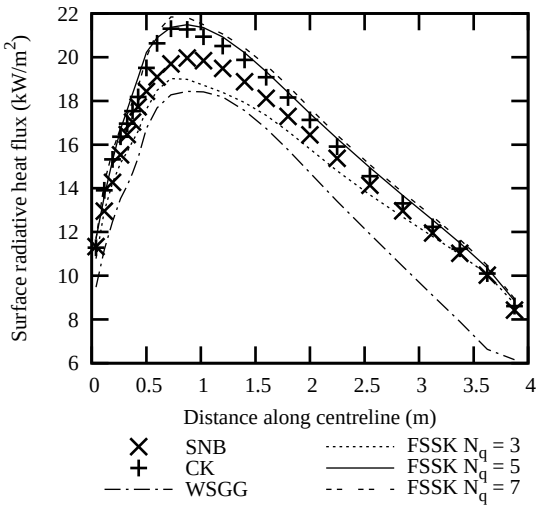

(b) Surface radiative heat flux calculations along the wall line (0m,1m,z).

Figure 6: Results for the FSSK on the first case.

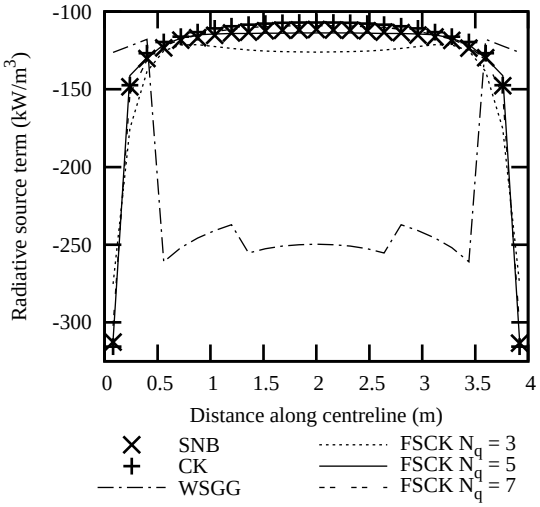

(a) Radiative source term calculations along the centreline.

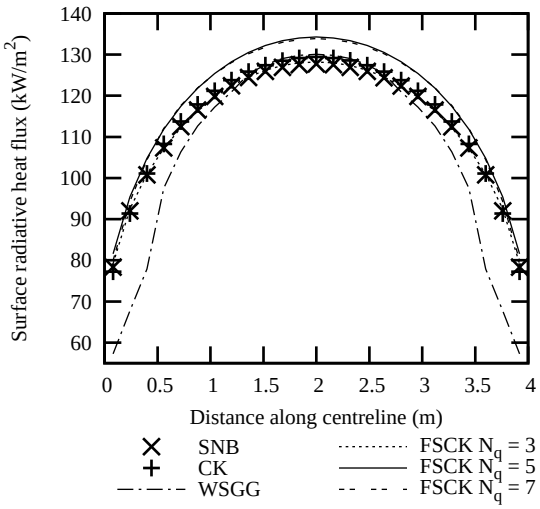

(b) Surface radiative heat flux calculations along the wall line (0m,1m,z).

Figure 7: Results for the FSCK model on the second case.

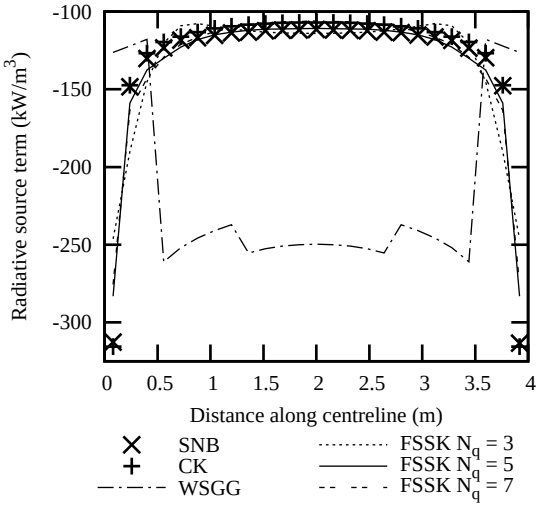

(a) Radiative source term calculations along the centreline.

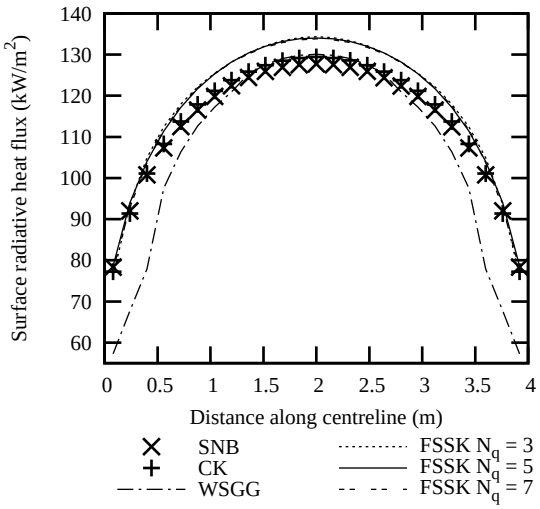

(b) Surface radiative heat flux calculations along the wall line (0m,1m,z).

Figure 8: Results for the FSSK model on the second case.

In contrast to the FSK models, the predictions from the WSGG method show significant disagreement with the benchmark data, as was reported previously by Porter et al. [9].

The results for the second case are illustrated in Figures 7 and 8. As with the first case, the plots represent the calculated values for radiative source term along the centreline of the enclosure parallel to the z-axis, and the radiative heat flux on the wall along the line (0m,1m,z). The two benchmark models show reasonable agreement in the second case, however there is still some disagreement in the source term and surface flux. Similarly to the first case, the predictions of the FSCK and FSSK models only show a minor difference between using five and seven quadrature points, further highlighting a five-point scheme as being optimal for these models under oxyfuel conditions.

Unlike the first case, the two FSK models provide visibly different results in the calculation of the radiative source term. The major departure between the two models is near the walls of the domain, where FSSK model underpredicts the magnitude of the source term. As the number of quadrature points increases in the FSSK model, this divergence from the benchmark data increases. The heat flux prediction of the FSK models show very good agreement with each other, but over-predict the heat flux calculated by the narrow-band models. The heat flux calculated by the FSSK with only three quadrature points shows very good agreement with the more refined FSSK results, however this is not captured in the source term.

Unlike the first case, the disagreement between the SNB and FSK models in the heat flux calculation is not captured in the CK model, and this departure could be explained as an inaccuracy introduced in the assumptions

of the FSK models. It has been shown that FSK models can be inaccurate for pure CO_2 due to the inability to account for transparent regions of the absorption coefficient [16], however the concentration of CO_2 in the second case is less than the first case, while the agreement has worsened. As this is the case, it is expected that these inaccuracies are caused by the breakdown of the correlated and scaled assumptions in the widely varying mixture ratio across the domain.

There is a wide disagreement between the grey WSGG and the narrow-band models in the second case. The grey WSGG model fails to predict the source term both qualitatively and quantitatively. Furthermore, the discontinuities inherent in the parameters for the model are clearly visible in the derived results. The surface heat flux calculations show better agreement than the source term, however the results still show less agreement with the benchmark data than with the FSK models.

The results presented in this section have shown that the FSCK model demonstrates reasonable predictions in derived radiative quantities under challenging oxyfuel conditions. The FSSK model also performs well under these environments, but is generally outperformed by the FSCK model in the second case considered in this work. Both FSK models showed significantly better agreement than the standard grey WSGG model, and offer an improvement in the treatment of radiative properties for CFD calculations.

5. Conclusions

This study compared the performance of FSK models in predicting the radiative source term and surface heat flux against narrow-band predictions

across two different cases that represent potential oxyfuel conditions, and that challenge the inherent assumptions of the global models. The first case, which had a non-uniform temperature distribution with a constant gas-species composition, could be reasonably approximated with both FSK models, with little differences between the approaches. The second case, with significant variations in species concentrations at a constant temperature, proved to be more discriminating, and the FSCK model achieved better agreement with the benchmark data close to the walls. From the results in this work, the FSCK model with a five-point Gauss quadrature scheme is recommended for modelling radiation heat transfer in CFD calculations on an oxyfuel environment.

Acknowledgements

The authors would like to thank the European Community's Seventh Framework Programme RELCOM project (grant agreement n. 268191) for providing funding for this research. The authors would also like to thank Prof. Michael Modest for providing the Spectral Radiation Calculation Software (SRCS) that was used to generate the full-spectrum k-distribution parameters for this work.

References

[1] N. Aimard, M. Lescanne, G. Mouronval, C. Prèbendè, in: International Petroleum Technology Conference.

[2] L. Strömberg, G. Lindgren, J. Jacoby, R. Giering, M. Anheden,

U. Burchhardt, H. Altmann, F. Kluger, G.-N. Stamatelopoulos, Energy Procedia 1 (2009) 581 – 589. doi:10.1016/j.egypro.2009.01.077.

[3] T. Uchida, T. Goto, T. Yamada, T. Kiga, C. Spero, Energy Procedia 37 (2013) 1471 – 1479. doi:http://dx.doi.org/10.1016/j.egypro.2013.06.022.

[4] P. Edge, M. Gharebaghi, R. Irons, R. Porter, R. Porter, M. Pourkashanian, D. Smith, P. Stephenson, A. Williams, Chemical Engineering Research and Design 89 (2011) 1470 – 1493. doi:10.1016/j.cherd.2010.11.010.

[5] G. Scheffknecht, L. Al-Makhadmeh, U. Schnell, J. Maier, International Journal of Greenhouse Gas Control 5, Supplement 1 (2011) S16 – S35. doi:10.1016/j.ijggc.2011.05.020.

[6] L. Chen, S. Z. Yong, A. F. Ghoniem, Progress in Energy and Combustion Science 38 (2012) 156 – 214. doi:10.1016/j.pecs.2011.09.003.

[7] L. Wang, D. C. Haworth, S. R. Turns, M. F. Modest, Combustion and Flame 141 (2005) 170 – 179. doi:10.1016/j.combustflame.2004.12.015.

[8] T. Wall, Y. Liu, C. Spero, L. Elliott, S. Khare, R. Rathnam, F. Zeenathal, B. Moghtaderi, B. Buhre, C. Sheng, R. Gupta, T. Yamada, K. Makino, J. Yu, Chemical Engineering Research and Design 87 (2009) 1003 – 1016. doi:10.1016/j.cherd.2009.02.005.

[9] R. Porter, F. Liu, M. Pourkashanian, A. Williams, D. Smith, Journal of Quantitative Spectroscopy and Radiative Transfer 111 (2010) 2084 – 2094. doi:10.1016/j.jqsrt.2010.04.028.

[10] R. Demarco, J. Consalvi, A. Fuentes, S. Melis, International Journal of Thermal Sciences 50 (2011) 1672 – 1684. doi:10.1016/j.ijthermalsci.2011.03.026.

[11] P. Edge, S. Gubba, L. Ma, R. Porter, M. Pourkashanian, A. Williams, Proceedings of the Combustion Institute 33 (2011) 2709 – 2716. doi:10.1016/j.proci.2010.07.063.

[12] A. Pranzitelli, A. G. Clements, R. Porter, L. Ma, M. Pourkashanian, A. Duncan, in: Oxyfuel combustion conference 3.

[13] L. Pierrot, A. Soufiani, J. Taine, Journal of Quantitative Spectroscopy and Radiative Transfer 62 (1999) 523 – 548. doi:http://dx.doi.org/10.1016/S0022-4073(98)00125-3.

[14] M. Denison, B. Webb, Journal of Quantitative Spectroscopy and Radiative Transfer 50 (1993) 499 – 510. doi:10.1016/0022-4073(93)90043-H.

[15] V. P. Solovjov, B. W. Webb, Journal of Heat Transfer 133 (2011) 042701. doi:10.1115/1.4002775.

[16] H. Chu, F. Liu, J.-L. Consalvi, Journal of Quantitative Spectroscopy and Radiative Transfer 143 (2014) 111 – 120. doi:http://dx.doi.org/10.1016/j.jqsrt.2014.03.013, special Issue: The Seventh International Symposium on Radiative Transfer.

[17] F. Liu, Journal of heat transfer 121 (1999) 200–203.

[18] L. Rothman, I. Gordon, R. Barber, H. Dothe, R. Gamache, A. Goldman, V. Perevalov, S. Tashkun, J. Tennyson, Journal of Quantit-

ative Spectroscopy and Radiative Transfer 111 (2010) 2139 – 2150. doi:10.1016/j.jqsrt.2010.05.001.

[19] W. Malkmus, Journal of the Optical Society of America 57 (1967) 323–329. doi:10.1364/JOSA.57.000323.

[20] J. Taine, A. Soufiani, volume 33 of *Advances in Heat Transfer*, Elsevier, 1999, pp. 295 – 414. doi:http://dx.doi.org/10.1016/S0065-2717(08)70306-X.

[21] W. L. Godson, Quarterly Journal of the Royal Meteorological Society 79 (1953) 367–379. doi:10.1002/qj.49707934104.

[22] C. P. Thurgood, A. Pollard, H. A. Becker, Journal of heat transfer 117 (1995) 1068–1070.

[23] M. F. Modest, Radiative heat transfer, second edition ed., Academic Press, 2003.

[24] P. Rivière, A. Soufiani, International Journal of Heat and Mass Transfer 55 (2012) 3349 – 3358. doi:10.1016/j.ijheatmasstransfer.2012.03.019.

[25] M. F. Modest, R. J. Riazzi, Journal of Quantitative Spectroscopy and Radiative Transfer 90 (2005) 169 – 189. doi:10.1016/j.jqsrt.2004.03.007.

[26] M. F. Modest, Journal of Quantitative Spectroscopy and Radiative Transfer 76 (2003) 69 – 83. doi:10.1016/S0022-4073(02)00046-8.

[27] M. F. Modest, H. Zhang, Journal of Heat Transfer 124 (2002) 30–38. doi:10.1115/1.1418697.

[28] J. Cai, M. F. Modest, Journal of Quantitative Spectroscopy and Radiative Transfer 141 (2014) 65 – 72. doi:http://dx.doi.org/10.1016/j.jqsrt.2014.02.028.

[29] S. A. Tashkun, V. I. Perevalov, Journal of Quantitative Spectroscopy and Radiative Transfer 112 (2011) 1403 – 1410. doi:http://dx.doi.org/10.1016/j.jqsrt.2011.03.005.

[30] P. Rivière, A. Soufiani, J. Taine, Journal of Quantitative Spectroscopy and Radiative Transfer 48 (1992) 187 – 203. doi:10.1016/0022-4073(92)90088-L.

[31] T. F. Smith, Z. F. Shen, J. N. Friedman, Journal of Heat Transfer 104 (1982) 602–608.